Numerical analysis of electro-fluid-flexible body interaction

Author

Muhammad Asfandyar Arshad

Registration Number

172325

Supervisor

Dr. Emad Uddin

DEPARTMENT

SCHOOL OF MECHANICAL & MANUFACTURING ENGINEERING

NATIONAL UNIVERSITY OF SCIENCES AND TECHNOLOGY

ISLAMABAD

November, 2019

Numerical analysis of electro-fluid-flexible body interaction

Author

Muhammad Asfandyar Arshad

Registration Number

172325

A thesis submitted in partial fulfillment of the requirements for the degree of

MS Mechanical Engineering

Thesis Supervisor:

Dr. Emad Uddin

Thesis Supervisor's Signature: _____

DEPARTMENT

SCHOOL OF MECHANICAL & MANUFACTURING ENGINEERING

NATIONAL UNIVERSITY OF SCIENCES AND TECHNOLOGY,

ISLAMABAD

November, 2019

Declaration

I certify that this research work titled "*Numerical analysis of electro-fluid-flexible body interaction"* is my own work. The work has not been presented elsewhere for assessment. The material that has been used from other sources it has been properly acknowledged / referred.

Signature of Student

Muhammad Asfandyar Arshad

172325

THESIS ACCEPTANCE CERTIFICATE

Certified that final copy of MS thesis written by Mr. Muhammad Asfandyar Arshad Registration No.172325, of SMME has been vetted by undersigned, found complete in all respects as per NUST Statutes / Regulations, is free of plagiarism, errors, and mistakes and is accepted as partial fulfillment for award of MS degree. It is further certified that necessary amendments as pointed out by GEC members of the scholar have also been incorporated in the said thesis.

Signature: _____

Name of Supervisor: Dr. Emad Uddin

Date: _____

Signature (HOD): _____

Date: _____

Signature (Principal): _____

Date: _____

Plagiarism Certificate (Turnitin Report)

This thesis has been checked for Plagiarism. Turnitin report endorsed by Supervisor is attached.

Signature of Student

Muhammad Asfandyar Arshad

Registration Number

172325

Signature of Supervisor

Copyright Statement

- Copyright in text of this thesis rests with the student author. Copies (by any process) either in full, or of extracts, may be made only in accordance with instructions given by the author and lodged in the Library of NUST School of Mechanical & Manufacturing Engineering (SMME). Details may be obtained by the Librarian. This page must form part of any such copies made. Further copies (by any process) may not be made without the permission (in writing) of the author.
- The ownership of any intellectual property rights which may be described in this thesis is vested in NUST School of Mechanical & Manufacturing Engineering, subject to any prior agreement to the contrary, and may not be made available for use by third parties without the written permission of the SMME, which will prescribe the terms and conditions of any such agreement.
- Further information on the conditions under which disclosures and exploitation may take place is available from the Library of NUST School of Mechanical & Manufacturing Engineering, Islamabad.

Acknowledgements

I am thankful to my Creator Allah Subhana-Watala to have guided me throughout this work at every step and for every new thought which You setup in my mind to improve it. Indeed I could have done nothing without Your priceless help and guidance. Whosoever helped me throughout the course of my thesis, whether my parents or any other individual was Your will, so indeed none be worthy of praise but You.

I am profusely thankful to my beloved parents who raised me when I was not capable of walking and continued to support me throughout in every department of my life.

I would also like to express special thanks to my supervisor Dr Emad Uddin for his help throughout my thesis and also for CFD and Advance Fluid Dynamics courses which he has taught me. I can safely say that I haven't learned any other engineering subject in such depth than the ones which he has taught.

I would also like to thank Dr.Muhammad Sajid, Dr. Zaib Ali and Dr. Samiur Rahman Shah for being on my thesis guidance and evaluation committee and express my special thanks to them for their help.

Finally, I would like to express my gratitude to all the individuals who have rendered valuable assistance to my study.

Dedicated to my exceptional parents and adored siblings whose tremendous support and cooperation led me to this wonderful accomplishment.

Abstract

A conventional piezoelectric flag is placed downstream of D the cylinder to study electro-fluid-structure interaction between the flag and the vortices generated by the D cylinder. The energy harvesting capability and dynamics of flow structure interaction is studied. The flow patterns associated with the piezoelectric flag and the dynamic response for stream wise, span wise distances are studied. The dynamic response of the flag into different modes of vibration corresponding to different states, amplitudes and frequencies has also been observed. Simulations indicate that large energy harvesting efficiency is achieved over a range of stream wise and span wise distances and there is higher value of voltage generation when there is lock in between vortex sheet fluctuations and flag vibration. The piezoelectric flag generate more energy when there is strong interaction between vortices and the flag flutter. Large amplitude flutter and more bending of the flag corresponds to promising energy harvesting efficiency of the flag. At stream wise distances 1.2-2 and the voltage generation of the piezoelectric material is increased irrespective of the span-wise distance.

Key Words: *Immersed boundary method, piezoelectric, energy harvesting eel, fluid structure interaction,*

Table of Contents

List of Figures

CHAPTER 1: INTRODUCTION

The research work presented below is the numerical analysis of flexible piezoelectric eel in the presence of D cylinder as a bluff body. The forced vibration of flexible filament in the wake of the bluff body is studied and results are presented in the research work.

1.1 Background, Scope and Motivation

The limitation of fossil fuels, the dependency of human race on the energy driven devices and environmental impact of fossil fuels had influenced scientist to devise new techniques and develop new methods in order to successfully extract the sustainable energy from other natural resources. Wind turbines, hydro turbines, extracting energy from the wave motion are some sources of extracting renewable energy. Latest development on the research of fluid structure interaction and invention of some smart materials has allowed scientists to develop new methods of low cost and effective energy generation methods.

The flapping dynamics of the flexible-flag in the presence of flow-induced instability has been studied previously in many numerical, experimental and analytical studies.(Alben, 2009; Alben & Shelley, 2008; W.-X. Huang & Sung, 2009; L. Tang, Païdoussis, & Jiang, 2009; Uddin, Huang, & Sung, 2013; Zhang, Childress, Libchaber, & Shelley, 2000). The dynamics of flexible body interaction is a conventional example of fluid structure interaction (FSI) in which the impact on the flexible body in the presence of fluid is studied. This study also laid out foundation of many naturally occurring phenomenon like fluttering of wings of insects and Birds (Ishihara, Horie, & Denda, 2009; Lighthill, 1975; Shoele & Zhu, 2015), wing fluttering of aircraft (D. Tang, Yamamoto, & Dowell, 2003), and snoring in humans(Nandwana, Ziaei, & Hansen, 2015; Pirnar, Dolenc-Grošelj, Fajdiga, & Žun, 2015) and energy harvesting applications(Doaré & Michelin, 2011; Dunnmon, Stanton, Mann, & Dowell, 2011; Giacomello & Porfiri, 2011; Guo, 2000; Michelin & Doaré, 2013; Shoele & Mittal, 2016).

In the dynamic study of immersed flexible plate in the axial flow, beyond the critical velocity the pressure forces destabilize the flexible plate dominates the structural rigidity and stabilizing effect of the plate, this results in the unstable flutter of the flexible plate (Paidoussis, 1998; Peng & Zhu, 2009; Shelley & Zhang, 2011). The exact value of this critical velocity entirely depends

on the structural properties like bending rigidity and density of the flexible plate and can be adjusted to the desired value to obtain that unstable flutter at low critical velocity. This unstable behavior of the flexible plate results in the self-sustained high amplitude flutter(Alben & Shelley, 2008; Michelin, Smith, & Glover, 2008) which can be used to generate a minimal amount of energy using piezoelectric patches attached to it(Akcabay & Young, 2012; Allen & Smits, 2001).

To determine the exact amount of energy that can be harvested using piezoelectric material an advance research has to be incorporated to study the intrinsic properties and their limits to optimize the energy harvesting efficiency of the piezoelectric filament. The coupling of fluid-solid and electrical system can be described in detail in theory and numerical analysis and the conversion mechanism from fluid solid to electrical energy must be explained in detail. In order to understand how much energy is dissipated a simpler model was developed which comprises of structural damping and assesses the capability of piezoelectric material to generate energy by flapping (Singh, Michelin, & De Langre, 2012a, 2012b; L. Tang et al., 2009). According to these researchers increasing the damping increases the energy dissipation of the system but re-stabilize the system early thus reducing the energy harvesting efficiency of the system. This the simplest method and easy to implement but it has some gaps to cover as it suppose that the energy is dissipated immediately, and cannot explain the dynamics of coupling of electrical and structural system.

When the elastic body is placed in a uniform axial flow, the body exhibits a transition from its steady state vibration to a self-sustained large amplitude flutter. The dynamics of the flutter may vary from chaotic in nature to simple periodic fluttering(Alben & Shelley, 2008; Connell & Yue, 2007; Virot, 2015). The energy is generated by the piezoelectric material when deflection/vibration is produced in it by applying any kind of stress and force(Kim, Kim, & Kim, 2011). It possible to maximize the energy produced from the piezoelectric material by carefully parameterizing the conditions and piezoelectric material properties of the filament. The piezoelectric properties can only be varied during the manufacturing process of the flag; the fabrication of flag must be done very precisely in order to extract as much energy as possible(Anton & Sodano, 2007). The flow velocities also play an important role in order to effectively maximize the generated voltage from a vibrating piezoelectric material. Although different vibration modes need to be studied in order to carefully determine that which mode of vibration is the most unstable energetic fluttering mode(Uddin et al., 2013). A bluff body can

also be placed in front of the flag in order to generate enough downstream disturbances that there is no need of adjustment of structural and energy producing properties of the piezoelectric flag(Akaydin, Elvin, & Andreopoulos, 2010).

Previously,(Doaré & Michelin, 2011) proposed fully fluid-structure-electric model in which they used piezoelectric patched flexible plate in the axial flows. They studied the effect of coupling on the linear stability of 2D piezoelectric plate and its impact of the energy transfer efficiency of the piezoelectric filament. They explained the role of mass ratio and tuning of fluid-structure-electric characteristics on the piezoelectric energy harvesting, and found out that in the presence of large fluid loading the piezoelectric coupling was destabilized due to the negative energy waves of the damped system. They further extended their work and studied the effect of key parameters like non-dimensional velocity, inertia ratio,tuning ratio and the coupling coefficient. They also confirmed their previous study regarding impact on the energy transfer efficiency by the destabilization due to damping(Michelin & Doaré, 2013). Many studies had also been done regarding the inverted piezoelectric flag in which the leading edge of the flag is set free and trailing edge is fixed. Both experimental and numerical models had been studied by varying the size of the flag, bending coefficient, tuning coefficient, piezoelectric coupling coefficient and non-dimensional flow velocity.

1.2 Fluid Dynamics and Flutter instability

When a flag is placed in the fluid it vibrates or stays at a position. This behavior of the flag is due to the competition between rigidity of the flag and pressure applied on the flag by the flowing fluid around the flag. The rigidity tends to keep the flag in the position of static equilibrium while surrounding fluid pushes the plate away from its equilibrium position.

In the flow induced vibrations such as flow over and airfoil, fluctuation of cylinder in the presence of vortex interactions and flow interaction on blades of wind turbine. All these interactions are rigid body interaction involving a limited number of degrees of freedom, but in case of flag flutter large deformations are produced and thus large number of degrees of freedom should be incorporated. The behavior of flag in the fluid flow vibration not only depend on the velocity and pressure variation in the fluid but also on the structural properties o like its material properties, dimension and rigidity etc. While modeling such a system involving such large

number of degree of freedoms a strong coupling between the fluid and the structure should be incorporated to solve the problem.

Previously many experimental studies have been done regarding this work (Taneda, 1968) while theoretical work is done using potential flow theory (Kornecki, Dowell, & O'brien, 1976; Wu, 1961). Due to recent inventions of powerful computational tools and flow visualization techniques this field of flutter instability have gain a lot of interests of the researchers and scientist, working on both structural mechanics and fluid dynamics. This work can be extended to different scenarios from fluid structure dynamics of single flag to multiple flags or including some bluff body to determine the interaction of fluid and body.

1.3 Dynamics of flag in a uniform flow

Many scientists have studied the dynamics of flag in the presence of uniform flow (Eloy, Souilliez, & Schouveiler, 2007; L. Huang, 1995; Shelley & Zhang, 2011). The motion of a filament in flow generated by soap film is studied by (Zhang et al., 2000). It was found out that the filament is behaving in 2 fundamental states one state is stretched when length of flag is small and the other is flapping state is considered when the length is large enough so that the flag can flap. They also studied the behavior of the flapping filament like its amplitude and frequency with filaments length and identified the phenomena of hysteresis by increasing or decreasing the length of the filament. The fluttering of the paper by using different materials and their theoretical models representing the observations in the experimental study was also studied. In these studies the relationship between speed of flutter and the mass ratio or fluid and solid's inertial ratio is taken into the account (Watanabe, Suzuki, Sugihara, & Sueoka, 2002)**).** Other experimental works studied wide variety of flutter materials such as paper, fabrics, flags an metals in wind tunnel, they studied stability and critical dynamic behavior of these flags (Eloy, Kofman, & Schouveiler, 2012; Gibbs, Wang, & Dowell, 2012; Virot, Amandolese, & Hémon, 2013).

In the past few years due to increased computational technology large amount of numerical work has done regarding the flapping dynamics of flag and flexible plate. The numerical method using immersed boundary method and implementing it by using direct numerical simulation was developed to replicate the experimental study (Zhu & Peskin, 2002). Another numerical approach using arbitrary Lagrangian and Eulerian (ALE) was developed to complement the

experimental study. Both the numerical solutions and experimental results are in good qualitative agreement with each other

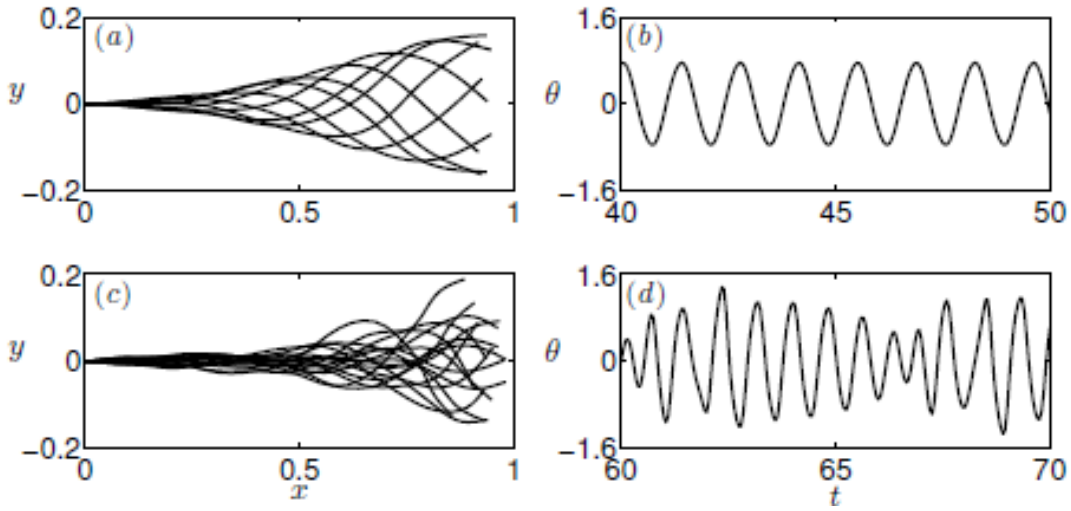

FIGURE 1. The flexible flag in uniform flow

As there are many uses of numerical simulation there are some disadvantages, it take a lot of time and not suitable when Reynolds numbers are high. Despite of high computing power systems the numerical simulations are still very time consuming. A very simplified model in always in need to carry out the complex simulation in less time and requiring less computational power. A variety of simplified model are developed and used by the researchers in order to carry out complex simulations in less time. Euler Bernoulli beam model is one of the best models to study inextensibility of flag and inviscid and incompressibility of the flow. The vortex sheet method to study fluid forcing and the flow field around the flapping flag is studied by the (Alben & Shelley, 2008). They found out that the two states of the flag i.e. stretched state and flapping state is divided by the undefined amplitude and frequency, which appears in the flow when there are relatively larger velocities. (Michelin, Smith, & Glover, 2008) used point vortex model and found out the presence of chaotic state of filament.

The previous studies including experimental and numerical are excellent oft understanding the dynamics of 2D flag. However they cannot fully explain the flag dynamics as they consider the flag to be 2d having infinite span which is unrealistic. Flag span should also have an effect on the flapping dynamics of the flag. Many studies have been done which explain the flapping dynamics of the 3D flag. In one of the study it is found out that flag span has significant influence on the flapping dynamics and stability of the flag. For fixed length the onset flapping

take place at lower velocity rather than on higher velocities (Eloy et al., 2007). These results are supported by the experimental study conducted by (Gibbs et al., 2012). In his study the flag dynamics is study by experimental work while the flag stability is done using euler Bernoulli which defines the flag and fluid loading is done by using vortex lattice model (Tang & Paı, 2007). The lighthill theory or (LAEBT), which was first developed to study the fish schooling (Candelier, Boyer, & Leroyer, 2011; Lighthill, 1971), is recently used to study the 3D flapping flags (Eloy et al., 2012; Michelin & Doaré, 2013; Singh, Michelin, & De Langre, 2012). He did it by adding the drag terms that corresponds to the lateral flow induced separation due finite span of the flag. DNS techniques have also been developed for 3D simulations (Tian, Lu, & Luo, 2012).

The effects of wall are also studied in the uniform flow by various scientists. Usually 3 type of configurations are studied in these studies. The presence of a single rigid wall parallel to the flag plane was studied (Dessi & Mazzocconi, 2015; Nuhait & Mook, 2010). The two rigid walls study parallel to the plane of flag was studied (Alben, 2015; Belanger, Paidoussis, & de Langre, 1995; Guo & Paidoussis, 2000). The presence of walls perpendicular to the flag's plane, therefore confined from sides of the flag. These walls have destabilizing effect on the flag, it means that confinement decreases the critical velocity of flag at which it behavior was stable. The flapping amplitude decreases after decreasing the channel wall distance from high value. This behavior is due to confinement of channel wall.(Alben, 2015).

1.4 Piezoelectricity

As the name suggests the piezoelectric materials voltage in response to the pressure or stress applied on them. These materials generate electric current as the deformation is produced in them as a result of stress. The piezoelectric material was discovered by (Curie & Curie, 1880) (Curie & Curie, 1880). Their study was only confined to the electric current generation form the deformation of the piezoelectric material which is called direct piezoelectric effect. Another effect of piezoelectric material was discovered by the French scientist name Garbriel Lippmann. He discovered that the piezoelectric material undergoes deformation under the influence of external electric charge(Lippmann, 1881). The mathematical argument regarding this was experimentally proved and concluded in the same year by (Curie & Curie, 1881).

In their work the Curie brother studied the naturally existing Quartz crystals. They concluded that the main reason behind generation of electric current from naturally existing piezoelectric material is the formation of natural dipoles within the material. This is the main phenomena which are applied to all existing piezoelectric materials. The formation of dipoles varies differently according to specific category of the material.(Ramadan, Sameoto, & Evoy, 2014)

After determining that electric dipoles generate electricity we can determine that how direct and inverse piezoelectric effects are produced. We can determine that how different parameters have effect on the piezoelectric energy generating capability of the material. The piezoelectric material is electrically neutral in the absence of stress and deformation which means that both the positive and negative electrode in the material are coinciding with each other. When the stress or pressure is applied on the filament the centers of positive and negative electrodes get stretched or compressed creating a field of current with in the material and generating the voltage difference. The conductive wire is connected to positive and negative electrodes of the material in order to transmit charge from material to external circuit. This is basis of direct piezoelectric effect of the piezoelectric material. Contrary to this concept an externally applied electric field has an impact

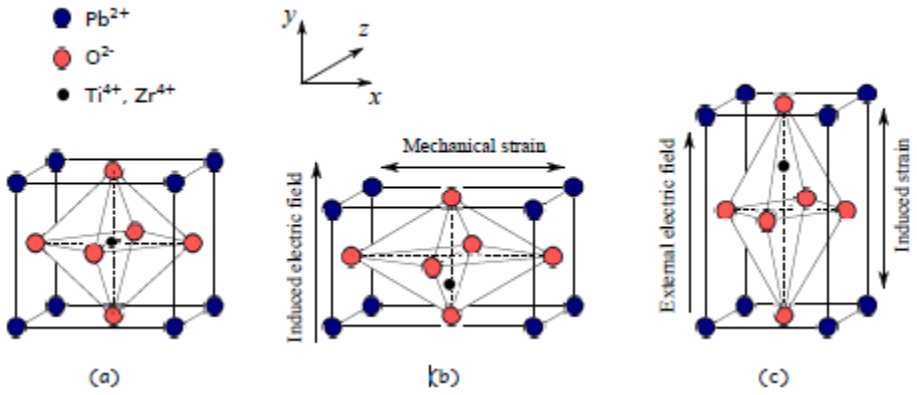

FIGURE 2. . (a)Cell Structure of piezoelectric material: (b) direct piezoelectric effect: (c) Inverse piezoelectric effect

on the neutral behavior of a piezoelectric material. The electric field will change the internal electrical dynamics of the piezoelectric material. In order to restore it original position and thus neutrality of the piezoelectric material the positive and negative electrode move in such a way that they come to their originally neutral positions, thus the material is mechanically deformed and stress in induced in the system producing inverse piezoelectric effect.

Consider the elementary crystal of piezoelectric crystal lead zirconate titanate (PZT) as shown in figure 3. The figure 3(a) shows the crystal in neutral form i.e. the positive and negative electrodes of the crystal are at center and same point. As the strain is applied on the structure figure 3(b) the centers of the crystal move away from each other in the vertical direction and generate the electric field which can be transmitted to external circuit. On the contrary if external electric potential is applied on the PZT crystal as shown in figure 3(c) the positive and negative electrodes move opposite to each other causing deformation inside the structure.

There are many four categories of piezoelectric materials that are described below.

1.4.1 Ceramics

The piezoelectric ceramics have excellent piezoelectric properties. The main advantage of piezoelectric ceramics is that they are made in the powder form and thus can be transformed into any type of geometric shape like disc, cylinders, plates or thin films. The piezoelectric properties of quartz are stronger than ceramics but conforming into any shape is considered very advantageous for ceramics piezoelectric materials. As they are ceramics with high brittleness so their application is also limited

1.4.2 Quartz

This is the naturally occurring kind of piezoelectric material and is in the form of crystals. It has strong piezoelectric properties along with high stiffness, low sensitivity to temperature and atmospheric conditions. These are used where more precision is required like in frequency control modules, electronic watches and microprocessor based equipment. They are less applicable to be used in places where high deformation is required. They cannot also be shaped into different shapes owing to their crystalline properties.

1.4.3 Polymers

Mostly used piezoelectric material is PVDF polyvinylidene Fluoride. Polymers have natural properties that they are very flexible in nature and are softer as compared to quartz and ceramics. They have weak piezoelectric properties but due to their flexibility they are used in variety applications. They are more mechanically stable as due to their flexibility. They usually come in

the form of thin filaments and can be transformed into desired lengths. Due to ability to sustain large deformations they are widely used in experimental research work regarding energy generation from piezoelectric materials.

1.4.4 Composite materials

The flexibility of polymers and rigidity of ceramics is incorporated is special type of piezoelectric material that are softer and flexible and at the same time have certain kind of rigidity. Due to these structural properties the composite piezoelectric material can be used in the studies where large deformation is required.

1.5 Energy harvesting form piezoelectricity

The property of piezoelectric material to convert mechanical deformation into electrical energy the piezoelectric material has been widely studied in applications like vibration suppression (Bisegna, Caruso, & Maceri, 2006; Ducarne, Thomas, & Deü, 2012; Thomas, Deü, & Ducarne, 2009).

The energy generation using piezoelectric material was being studied around two decades ago (Umeda 1996). The basic idea of this study is to convert vibrational energy source into an electrical energy through piezoelectric materials. A lot of work has been done in the past to improve the energy harvesting efficiency of the piezoelectric systems (Anton & Sodano, 2007; Caliò et al., 2014)

Energy harvesting from the flow can be done by using the non-uniformity of fluid structures and their forcing due to vortex induced vibration in the presence of bluff body (Allen & Smits, 2001; Pobering & Schwesinger, 2004).In the present work it a fully coupled fluid-solid-electric-coupled system is proposed in which flexible filament is placed in the wake of highly unsteady flow in the presence of D cylinder with flexible filament is covered with small piezoelectric patches (Doaré & Michelin, 2011).

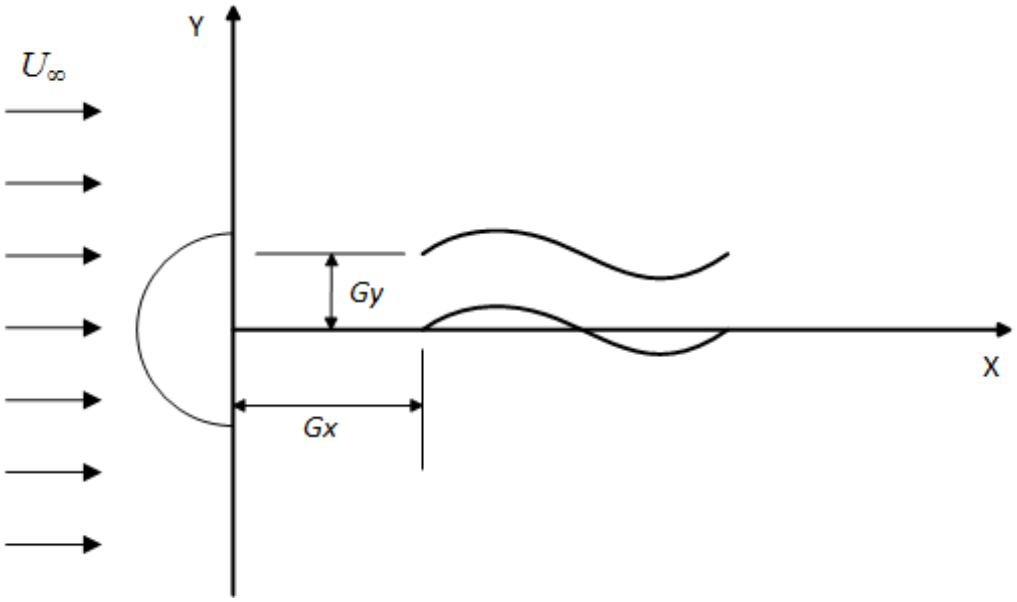

FIGURE 3. Schematic diagram

Recently (Shoele & Mittal, 2016) used this approach to understand the energy harvesting capability of inverted piezoelectric filament in uniform axial flows. The flapping dynamics of flag is studied by (Uddin & Sung, 2012) in which the flapping dynamics of flag in the uniform flow is studied, this work further extend the work to harvest energy by covering flexible filament with piezoelectric patches. All the previous work in which numerical simulation is done in order to study the energy harvesting capability of the piezoelectric flag used the stable flowing conditions with no induced fluctuation in the flow. The innovation of present work is using unsteady flow conditions in order to study the effect of vortices generated by the d cylinder on the flexible filament and changing the span-wise distance G_x and stream-wise distance G_y in order to study at which area in the wake of the bluff body the energy generation of the piezoelectric flag is maximum.

CHAPTER 2: ANALYTICAL MODELS AND NUMERICAL METHODOLOGY

2.1 Numerical methodology

A flexible flag in the wake of a D-shaped half cylinder was subjected to the two-dimensional viscous flow. A schematic diagram of the geometric configuration and the coordinate system is shown in figure 1.

The distance between the D-shaped half cylinder and the flexible flag was varied by adjusting the stream-wise gap distance "Gx". The head of the downstream flag was fixed under a simply supported boundary condition and the boundary condition for the free end was considered at the tails. The rigid D-shaped half cylinder is placed at the center (0,0) with diameter "D". The fluid domain was defined by an Eulerian coordinate system, and a separate Lagrangian coordinate system was applied to the flexible flag. The flexible flag in a viscous flow were modeled using an improved immersed boundary method(W.-X. Huang, Shin, & Sung, 2007), in which the governing equations of the fluid flow and the flexible flag was solved in each coordinate system, and the interactions among components was calculated using a feedback law.

The fluid motion was governed by the incompressible Navier-Stokes and continuity equations,

$$\frac{\partial \boldsymbol{u}}{\partial t} + \boldsymbol{u}\cdot\nabla\boldsymbol{u} = -\nabla p + \frac{1}{\mathrm{Re}}\nabla^2\boldsymbol{u} + \boldsymbol{f}\ , \qquad (1)$$

$$\nabla\cdot\boldsymbol{u} = 0, \qquad (2)$$

where $\boldsymbol{u}$ is the velocity vector, p is the pressure, $\boldsymbol{f}$ is the momentum force applied to enforce the no-slip conditions along the immersed boundary, and the Reynolds number Re is defined by $\mathrm{Re} = \rho_0 U_\infty L/\mu$, with ρ_0 the fluid density, U_∞ the free stream velocity, L the flag length, and μ the dynamic viscosity.

The flag motion was governed by

$$\frac{\partial^2 \boldsymbol{X}}{\partial t^2} = \frac{\partial}{\partial s}\left(T \frac{\partial \boldsymbol{X}}{\partial s} \right) - \frac{\partial^2}{\partial s^2}\left(\gamma \frac{\partial^2 \boldsymbol{X}}{\partial s^2} \right) - \boldsymbol{F} \qquad (3)$$

where s denotes the arc length, $\boldsymbol{X} = \boldsymbol{X}(s,t)$ the position, T the tension force, γ the bending rigidity and $\boldsymbol{F}$ the Lagrangian force exerted on the flexible flag by the fluid. Equation (3) was non-dimensionalized by the flag density ρ_1, the flag length L, and the free stream velocity U_∞. It should be pointed out that the tension force can be determined from the inextensibility condition of flag(W.-X. Huang et al., 2007), and the bending rigidity is defined as EI, with E the Young's modulus and I the second moment of area, which gives the non-dimensional value γ. The boundary conditions applied at the fixed end and the free end were

$$\boldsymbol{X} = \boldsymbol{X}_0, \ \frac{\partial^2 \boldsymbol{X}}{\partial s^2} = (0,0) \qquad \text{for the fixed end,} \qquad (4)$$

$$T = 0, \frac{\partial^2 \boldsymbol{X}}{\partial s^2} = (0,0), \ \frac{\partial^3 \boldsymbol{X}}{\partial s^3} = (0,0) \qquad \text{for the free end.} \qquad (5)$$

The interaction force between the flow and the structure was calculated using the feedback force by the relation

$$\boldsymbol{F} = \alpha \int_0^t (\boldsymbol{U}_{ib} - \boldsymbol{U})\, d\tau + \beta (\boldsymbol{U}_{ib} - \boldsymbol{U}), \qquad (6)$$

where α and β are large negative free constants -10^5 and -10^3, respectively in(W.-X. Huang et al., 2007), $\boldsymbol{U}_{ib}$ is the fluid velocity obtained by interpolation at the immersed boundary, and $\boldsymbol{U}$ is the velocity of the flag expressed by $\boldsymbol{U} = d\boldsymbol{X}/dt$. On the other hand, $\boldsymbol{X}_{ib}$ and $\boldsymbol{U}_{ib}$ denote, respectively, the position and velocity of the immersed boundary, which were determined using the local Eulerian fluid velocity, as expressed by

$$\boldsymbol{U}_{ib}(s,t) = \int_\Omega \boldsymbol{u}(\boldsymbol{x},t)\delta(\boldsymbol{X}(s,t) - \boldsymbol{x})d\boldsymbol{x}, \qquad (7)$$

Where δ ( ) denotes a smoothed approximation of the Dirac delta function, and Ω_f is the fluid region. Equation (8) provides an interpolation of the Eulerian fluid velocity at the Lagrangian points. In physics, equations (6) – (8) represent a stiff spring system. This system connected the Lagrangian points on the immersed boundary to the surrounding fluid particles.

After obtaining the Lagrangian force $\boldsymbol{F}$, the expression was transformed to the Eulerian form using the smoothed Dirac delta function,

$$\boldsymbol{f}(\boldsymbol{x},t)=\frac{\rho_1}{\rho_0 L_r}\int_\Gamma \boldsymbol{F}(s,t)\delta(\boldsymbol{x}-\boldsymbol{X}(s,t))ds\,. \qquad (8)$$

Where, $\rho=\frac{\rho_1}{\rho_0 L_r}$based on the non-dimensionalization steps, and Ω_s denotes the structure region. After discretization, the force was applied over a width of several grids, which supported the smoothed delta function.

The overall computational process, in which the present numerical algorithm was used to simulate the fluid–flexible body interactions, is summarized as follows:

(1) Initialize the computation parameters, the meshes, and the fluid and solid motions; set $\boldsymbol{X}_{ib}^0=\boldsymbol{X}^0$.

(2) At the nth time step, the fluid velocity $\boldsymbol{u}^n$ and the solid position $\boldsymbol{X}^n$ and velocity $\boldsymbol{U}^n$ are known. Interpolate the fluid velocity at the Lagrangian points to obtain $\boldsymbol{U}_{ib}^n$, and calculate the positions of the immersed boundary points $\boldsymbol{X}_{ib}^n$. Then calculate the Lagrangian momentum force $\boldsymbol{F}^n$.

(3) Map the Lagrangian momentum force onto the Eulerian grid. Obtain the updated fluid velocity field and pressure field.

(4) Substitute $\boldsymbol{F}^n$ into the flag motion equation and obtain the flag position at the new time step $\boldsymbol{X}^{n+1}$, as well as the velocity $\boldsymbol{U}^{n+1}=(\boldsymbol{X}^{n+1}-\boldsymbol{X}^n)/\Delta t$. Return to step 2 and march to the next time step.

The computational domain for the fluid flow ranged from -2 to 6 in the stream-wise (x) direction and from -4 to 4 in the span-wise (y) direction, both of which directions were normalized by the flag length. The Eulerian grid size for the fluid was 512×350 in the stream-wise and span-wise directions, respectively, and the Lagrangian grid size for each flag was 64. The Eulerian grid was uniformly distributed along the x direction, and it was uniform in the y direction for $-2\le y\le 2$, but stretched otherwise. The far-flow field was applied at the top and bottom boundaries as well as the inlet of the fluid domain, whereas the convective boundary condition was used at the outlet. The computational time step was set to 0.0005, which resulted

in a CFL number of 0.1. The validation of the flow solver employing the immersed boundary method, as well as the structure solver for the flag motion, has been provided in(W.-X. Huang et al., 2007)

2.2 Governing Equation structure-electric interaction

As assumed the surface of piezoelectric flag is covered with small patches which has length smaller than the length of actual flag as done by(Doaré & Michelin, 2011). It was further extended in the study of voltage generation of inverted flag by (Shoele & Mittal, 2016). The deformations produced at different points in the flag are coupled with electrical system. Local bending and compression of the mesh points of the flag result in the charge and voltage generation of the flag. The coupling between the charge per unit length *Q,* voltage *V(s,t)* and the deformation in the flag is expressed by the following equation.

$$Q(s,t) = cV + \lambda \frac{\partial^2 \boldsymbol{X}}{\partial s^2} \qquad (9)$$

C and λ is defined as linear capacitance of piezoelectric patch and the coupling coefficient respectively, which is the natural property of the piezoelectric patch.

Assuming the pure resistive circuit between charge *Q* and voltage *V*

$$\frac{\partial Q}{\partial t} = -\varsigma V \qquad (10)$$

ς relates to the linear conductivity coefficient between upper and lower piezoelectric patches which we assumed on the surface of the filament. According to (Michelin & Doaré, 2013) the moment *M* with respect to *s* and *t* is defined as

$$M(s,t) = -\gamma \frac{\partial^2 \boldsymbol{X}}{\partial s^2}.\boldsymbol{n} + \chi V \qquad (11)$$

According to Euler-Bernoulli assumption regarding thin flat plate (Audoly & Pomeau, 2010)

$$\zeta = \frac{\partial M}{\partial s} \qquad (12)$$

This is rate of change of total moment with respect to lagrangian coordinate *s*

$$\zeta = \frac{\partial M}{\partial s} = -\frac{\partial}{\partial s}\left(\gamma \frac{\partial^2 \boldsymbol{X}}{\partial s^2}\right).\boldsymbol{n} + \chi \frac{\partial V}{\partial s} \qquad (13)$$

By combining equation (3)-(13), and non-dimensionalising the equation we get

$$\frac{\Pi \partial V}{\partial t}\left(\frac{\partial^2 \boldsymbol{X}}{\partial s^2}.\boldsymbol{n} = -V - \Omega * \frac{\beta\sqrt{M^*}}{U^*} * \partial/\partial t\right) \qquad (14)$$

Where,

Reynolds number $Re = \frac{LU}{\nu}$

The inertial ratio between the fluid and structure $M^* = \frac{\rho L}{m_s}$

$$m_s = m_f - \rho * A_s$$

$$m_f = mass\ per\ unit\ length$$

$$A_s = area\ of\ flag$$

Free-stream velocity (non-dimensionalised) $U^* = UL * \sqrt{\frac{\rho L}{\gamma}}$

The coupling coefficient $\Omega = \frac{\lambda}{\sqrt{\gamma}}$

λ =The coupling coefficient

Tuning coefficient (electrical system) $\Pi = cU/\varsigma L$

$$\varsigma = linear\ conductivity$$

$$c = linear\ capacitance$$

2.3 ANSYS Computational Model

The piezoelectric equation is an expression that describes the relationship between the mechanical and electrical quantities of piezoelectric materials. This kind of piezoelectric equation is used in the ANSYS coupling solutions for the analysis about piezoelectric materials. In linear piezoelectricity, the equations of elasticity are coupled to the charge equation of electrostatics by means of piezoelectric constants:

$$\{S\} = [s^E].\{T\} + [d].\{E\}$$

$$\{D\} = [d]^t.\{T\} + [\varepsilon^T].\{E\}$$

Where $\{S\}$ is the elastic strain vector; $\{T\}$ is the stress vector (N/m^2); $\{D\}$ is the electric flux density vector (C/m^2); $\{E\}$ is the electric field intensity vector (V/m); $[S^E]$ is the compliance matrix evaluated at constant electric field, i.e. short circuit; $[d]$ and $[d]t$ are the piezoelectric strain coefficient matrix (C/N), and the superscript$\{t\}$is the matrix transpose.

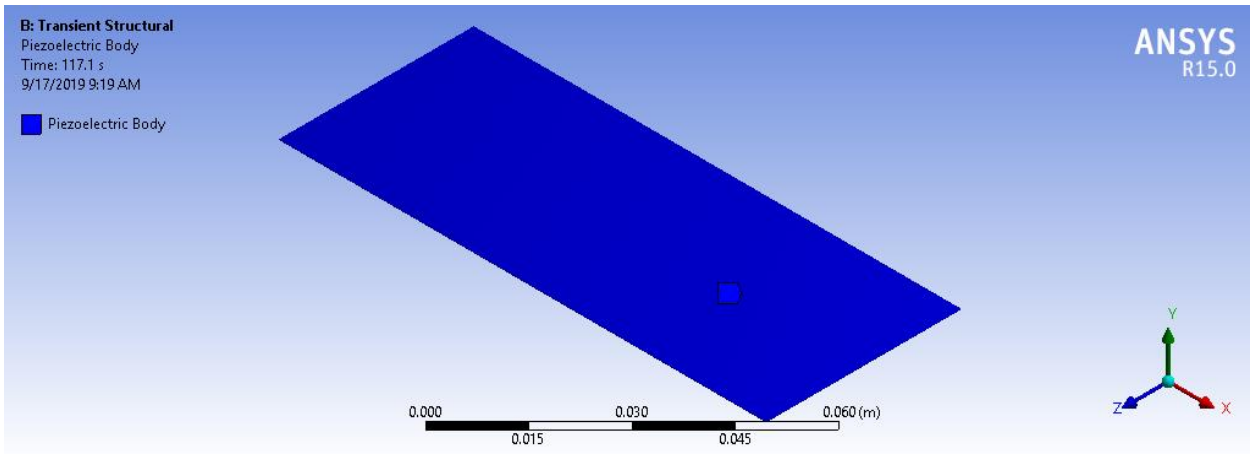

FIGURE 4. Model of Filament

CHAPTER 3: RESULTS & DISCUSSION

3.1 Effect of changing Span-wise and Stream-wise distances

In this section, we will focus on the role of changing the span wise distance G_y and stream wise gap G_x between the two flags on the dynamics of the flag place downstream. Span wise distance is changed from 0- 0.5 with increment of 0.25. Similarly the stream wise gap is increased from 0.5 to 2 for every span wise distance. Re=300, ρ=1 and ϒ=0.007 and these values are unchanged unless mentioned otherwise.

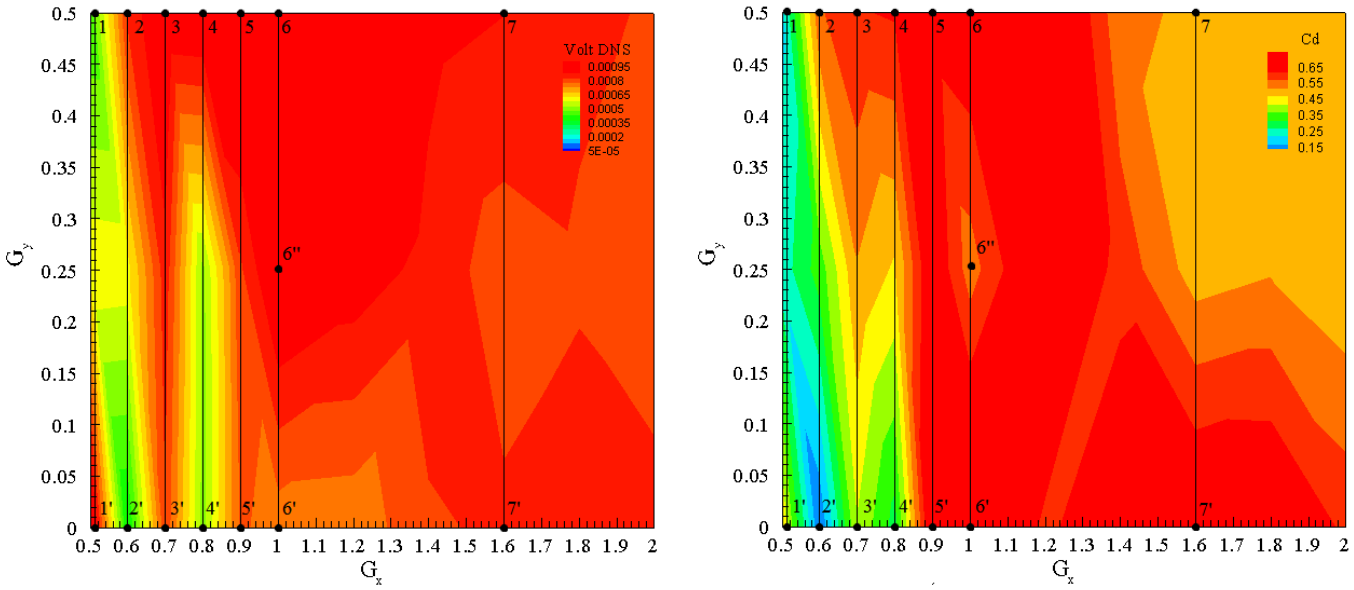

FIGURE 5. (a) Contour of Voltage (b) Contour of Coefficient of Drag

The dynamics of flag and flow patterns are used to study the flapping modes of the flag. The voltage generation capability of the piezoelectric flag is studies at all the stream wise and span wise gap distance. The coefficient of drag is also studied at these gap distances in order to study the effect of drag on the voltage generating capability of the flag. The flow patterns also play an important role in predicting the energy generation capability of the flag, which is explained in detail in this section. The deflected, biased and normal flapping modes are observed and these modes play an important role in predicting the drag and voltage generation of the flag.

The surface plot of voltage generation with the function of the G_x and G_y is shown in the figure 2 (a). It is clearly shown that voltage generated by the piezoelectric flag is increasing as the stream wise distance of the flag from the bluff body is increasing irrespective of the span wise distance.

This trend is also similar in case of drag coefficient as shown in figure 2 (b) but it can be seen that after stream wise distance of 1.2 changing the span-wise distance have small effect on the drag of the piezoelectric filament.

In the first case in the region where G_x=0.5 and G_y is changing from 0-0.5. The voltage produced by the piezoelectric material in decreasing as we increase the span wise distance Figure 2 (a). The behavior of coefficient of drag is also similar for this case figure 2 (b), but it can be seen that drop in voltage is not as prominent as drop in coefficient of drag. This drastic change in the value of coefficient of drag can be explained by the studying the fluid body interaction of vortices and flexible flag. The behavior of flag at span wise position G_y=0.0 and G_y=0.5 can be seen in the figure 3**.** It is quite clear from the figures that flag is not behaving normally when place at these span wise distance. Instead of horizontal motion with respect to the flow it is vibrating vertically downward (figure 3), thus the vortices generated by the D cylinder have minimal effect on the drag of the flag. Although the voltage is generated but this voltage is only due to fluctuation, as fluid around the flag is moving and causing vibrations in the flag. The amplitude of the tip displacement of the flag and its power spectrum complements the fact that energy transferred by the fluid to the flag as the span wise distance increases from 0 to 0.5 figure 4.

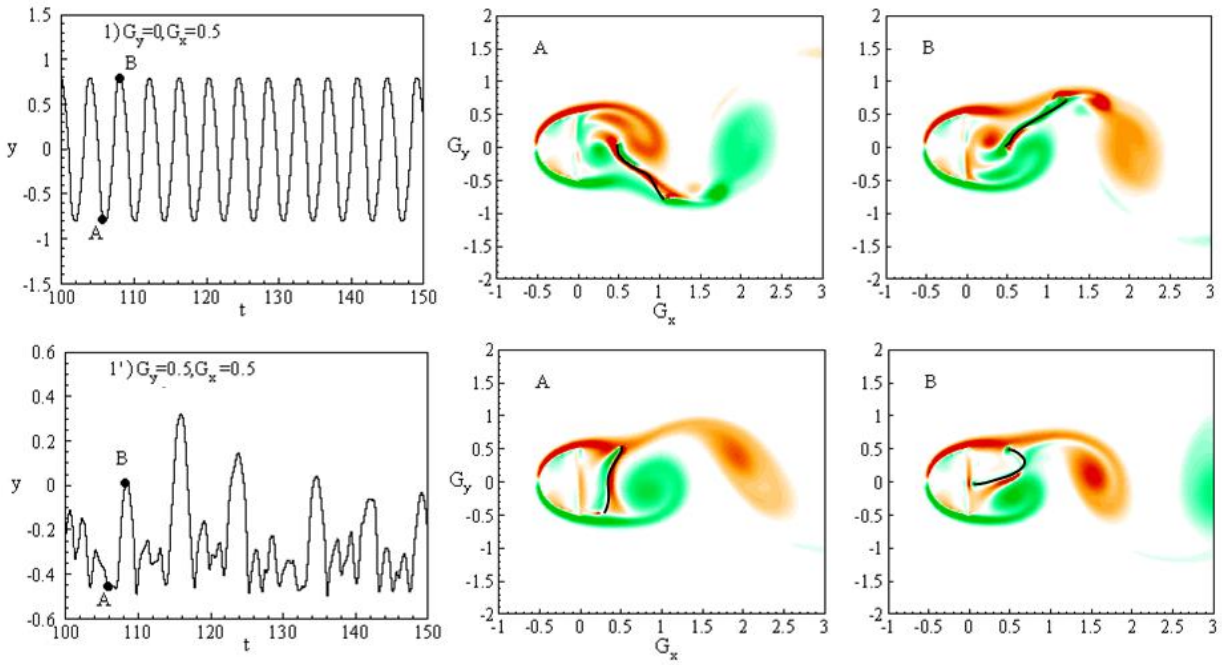

FIGURE 6. Vorticity contours around the flag for G_x=0.5 and G_y=0 and 0.5

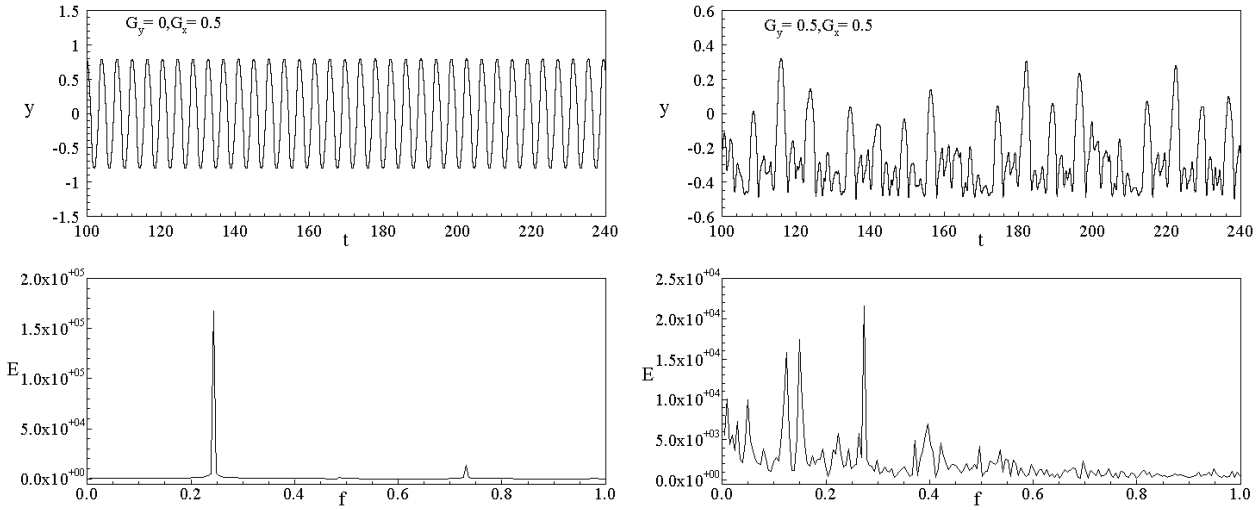

FIGURE 7. Frequency Plots for G_x=0.5 and G_y=0 and 0.5

In the region where flag is placed at constant G_x=0.6 with varying G_y, the voltage generating trend is similar to that of previous case where flag is placed at Gx=0.5 figure 2 (a)**.** The drag on the flag is minimum at point G_y=0 and it is increasing as G_y increases figure 2 (b). The very small value of drag at G_y=0 can be explained by looking in the fluid body interaction in figure 6**.** It can be seen in figure 5 that at G_y=0 and G_x=0.6 the free end of the flag gets attached to the fixed end, and the vibration continues. This mode of vibration is termed as deflected mode of

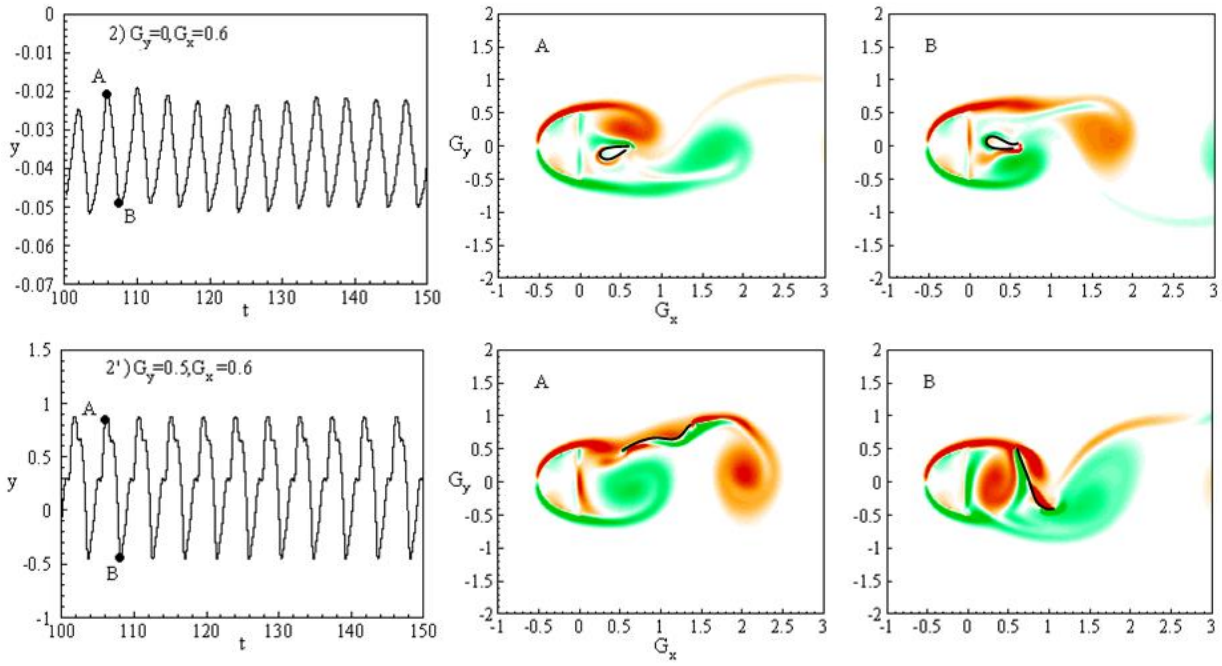

FIGURE 8. Vorticity contours around the flag for Gx=0.6 and Gy=0 and 0.5

vibration. Due to this behavior, the flag experiences very less drag due to vortex shedding, in fact it behaves another bluff body in the wake of D cylinder. When the span wise distance is increased at G_y=0.5 both the voltage generation and the drag on the flag is increased. At this point the interaction between vortices and the flexible flag is maximum thus imparting maximum energy to the flag generating ample amount of voltage (figure 6). The irregularities in the tip displacement time history and power spectrum further evident that the motion of the flag at this position corresponds to very less amount of energy transfer from fluid to the flag (figure 6).

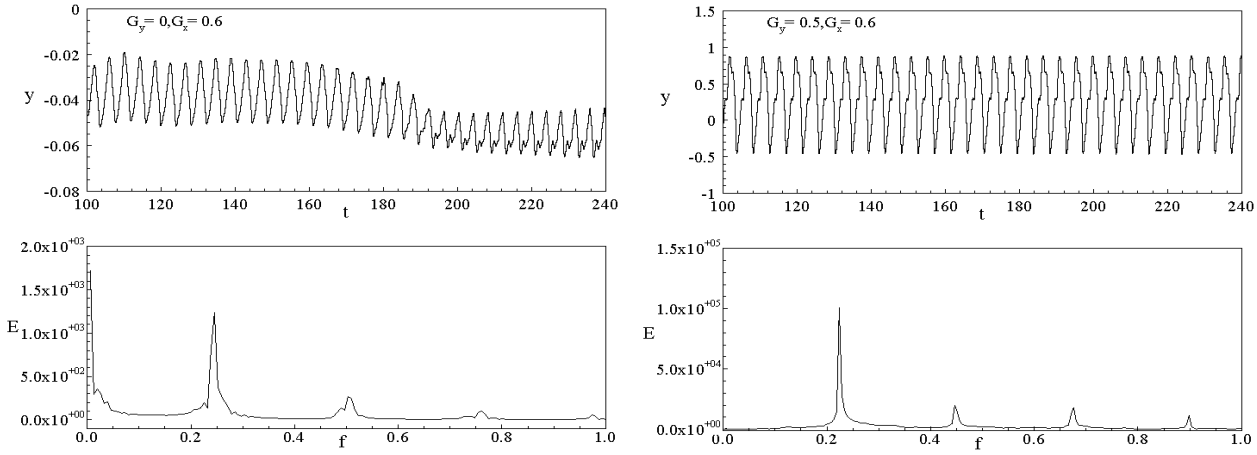

FIGURE 9. Frequency Plots for Gx=0.6 and Gy=0 and 0.5

When piezoelectric flag is placed at G_x=0.7, it can be seen that there is increase in the voltage as the span wise distance is increased figure 2 (a). There is also a relative increase in drag with the increase of span wise distance as shown in figure 2 (b)**.** The interaction of vortices with the flag at G_y=0 is shown in the figure 7. At this position, the flag exhibits biased mode of vibration, which mean that it is fluctuating conventionally as well as in deflected mode. Although the interaction between vortices and the flag is not proper but fluctuation of the flag in the vicinity of turbulent flow has large amplitudes, which results in the large value of the voltage. This behavior of the flag is quite evident in the figure 8 where vertical displacement of the flag is plotted w.r.t. time. The power spectrum of flag's displacement also shows the presence of multiple vibrating frequencies of the flag. At G_y=0.5 shown in the figure 7. It can be seen that at this point the clockwise rotating positive vortices fluctuates the whole flag, flag is under full influence of clockwise vortex while the anti-clockwise vortex hits the flag in the end just to give the bend to downward moving flag. Although the displacement and frequency plots at G_y=0.5 are smoother

than G_y=0 figure 8**.** This also indicates that if piezoelectric flag is vibrating smoothly with large frequency, it will produce more voltage and more have larger value of drag.

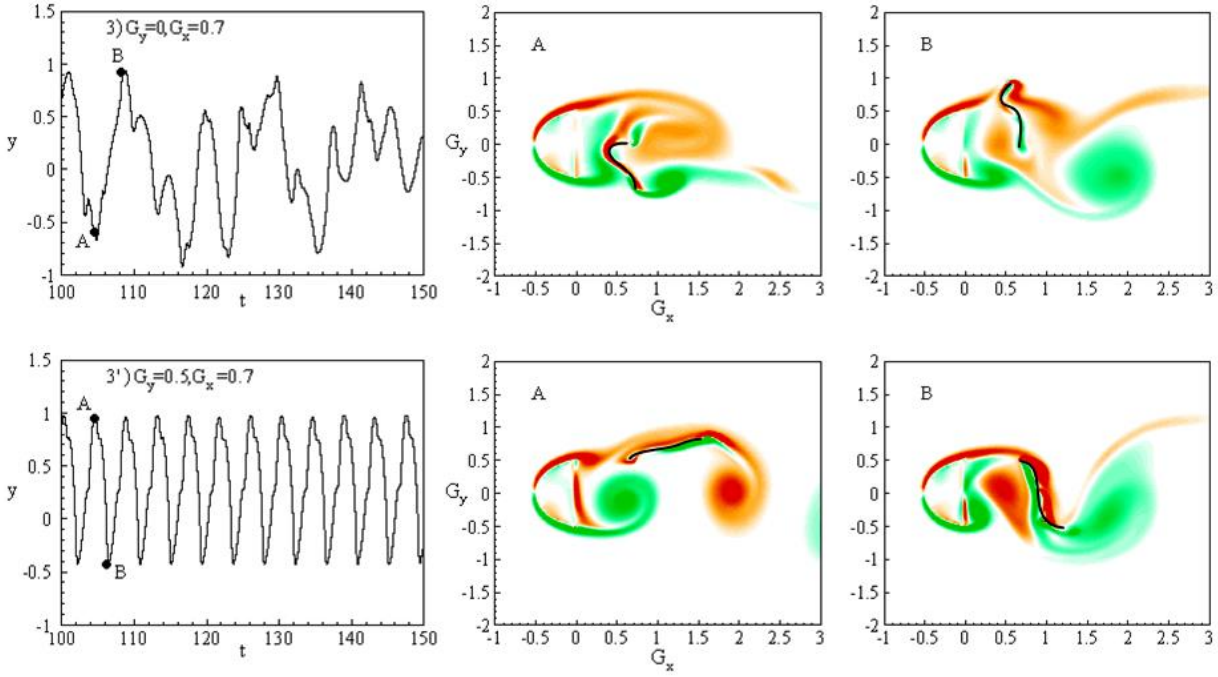

FIGURE 10. Vorticity contours around the flag for G_x=0.7 and G_y=0 and 0.5

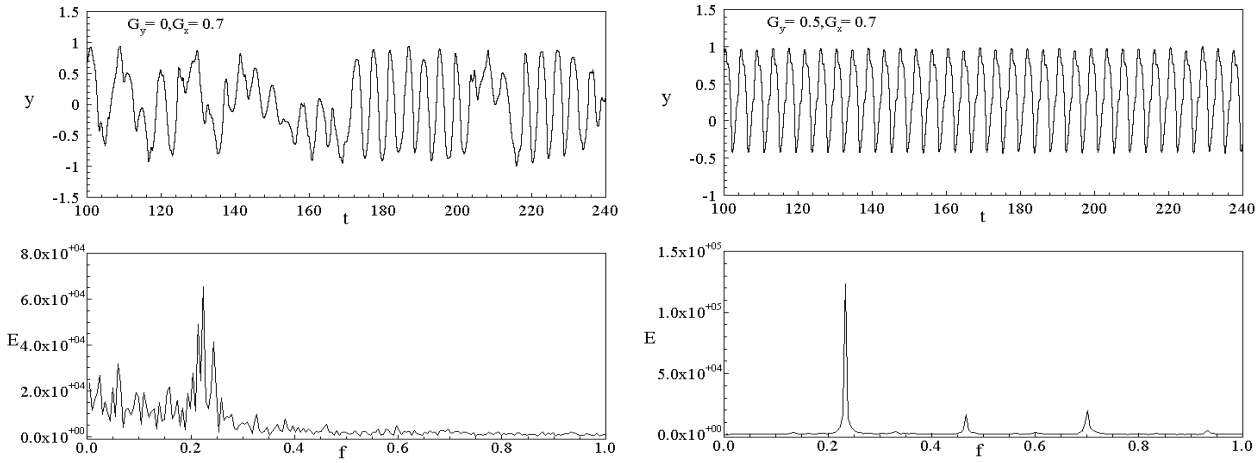

FIGURE 11. Frequency Plots for Gx=0.7 and Gy=0 and 0.5

When the flag is placed at G_x=0.8 with increasing span wise distance both value of drag and oltage shows an increasing trend. In this region, the fluctuation of the flag is conventional and lock in behavior is observed. The increase in the value of drag at G_y=0.5 is due to the total submergence of flag in the clockwise rotating vortex at lower position as shown in the figure 9.

This induces more bending in the middle section of the flag thus increasing the voltage generation of the flag.

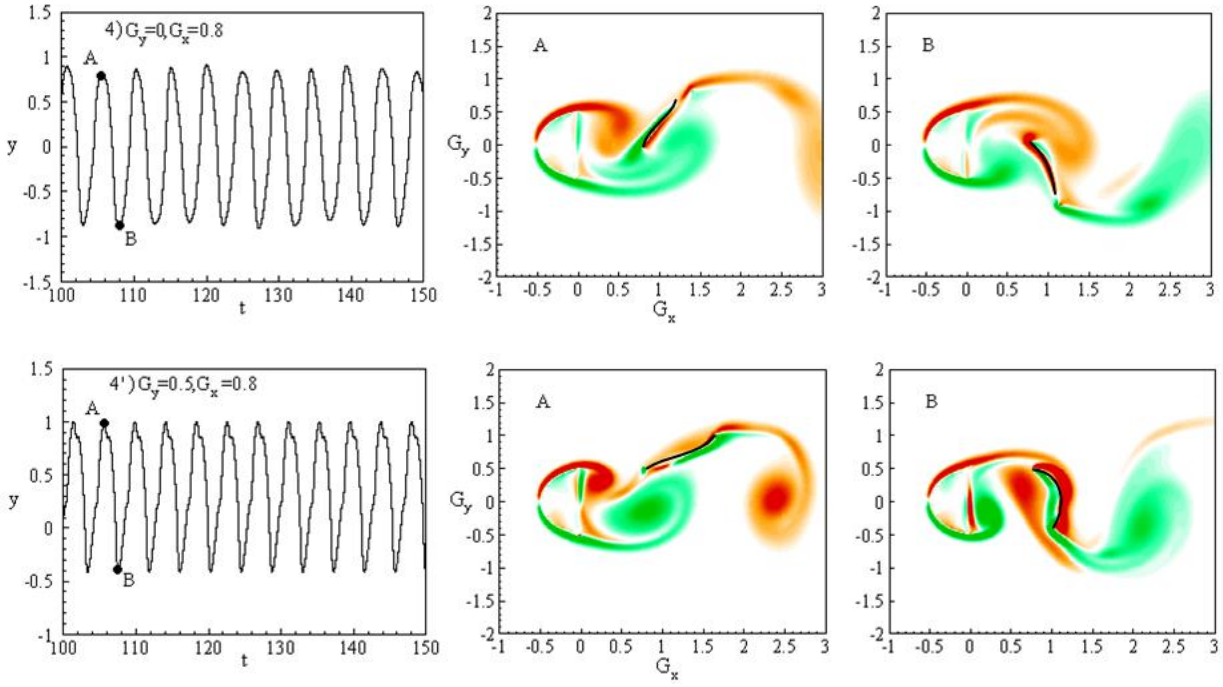

FIGURE 12. Vorticity contours around the flag for Gx=0.8 and Gy=0 and 0.5

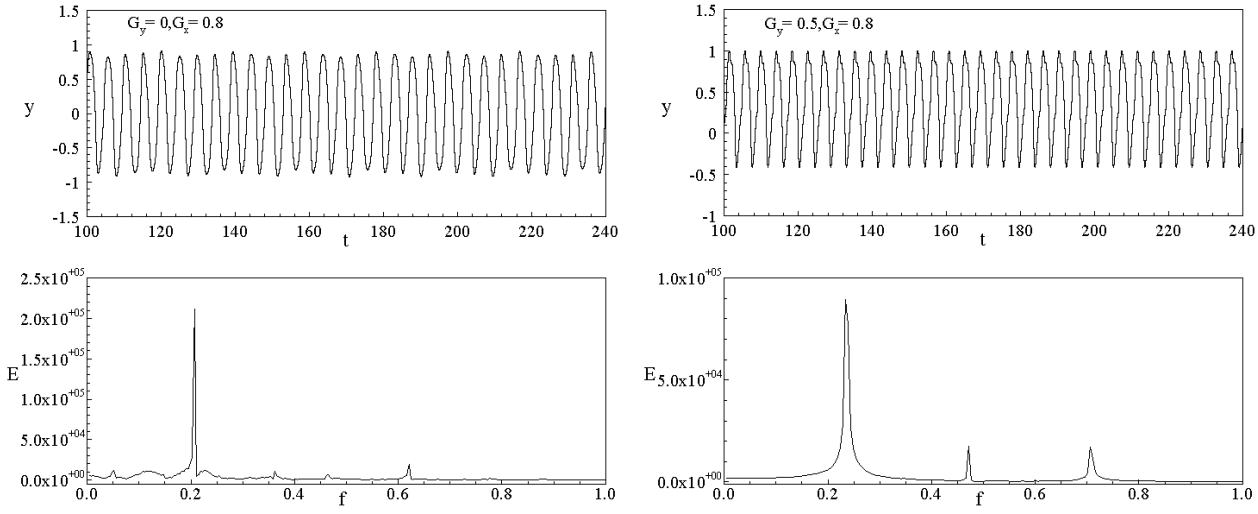

FIGURE 13. Frequency Plots for G_x=0.8 and G_y=0 and 0.5

On the other hand at G_y=0 the flag is straight as it is vibrating in the influence of the vortices. The frequency plots shows that there not much change in tip displacement (Figure 10) but change in voltage production is due to different vortex body interaction.

The results are somehow different from the trend when flag is placed at G_x=0.9 and there span wise distance is increased from 0-0.5. The voltage generated by the flag is increased when span

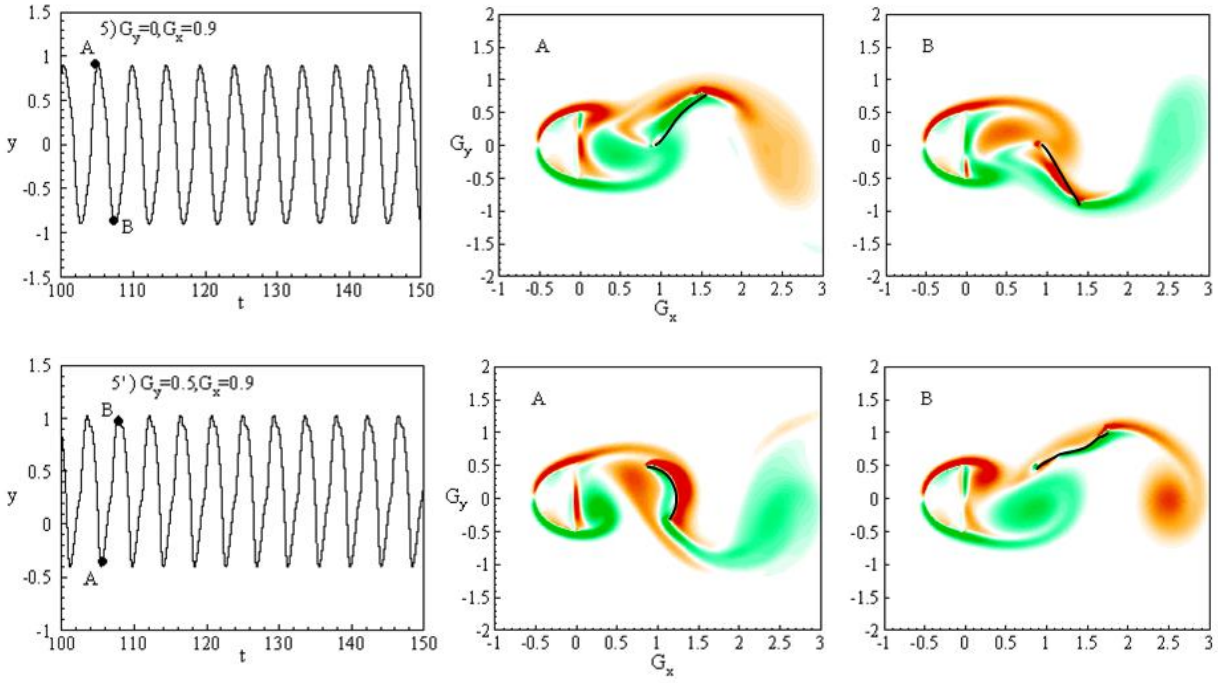

FIGURE 14. Vorticity contours around the flag for G_x=0.9 and G_y=0 and 0.5

wise distance is increased as shown in figure 2 (a)**,** but the drag is this region is almost the same. This trend of drag shown in figure 2 (b) can be understood by looking into the vortex body nteraction. At G_y=0 the pair of vortices are properly interacting with flag, the clockwise rotation vortex is pushing the flag down while the counter clockwise rotating vortex is pulling it up figure 11. On the other hand as the spanwise distance is increased the interaction of counter clockwise vortex coming from downward decrease with the flag and at G_y=0.9 only clockwise vortex interacts with whole flag, the counter clockwise vortex is just touching the flag in the end of it vibration and causing the flag to bend from the center figure 11. Due to this, the drag on the flag is only due to clockwise rotating vortex, but the voltage values are high because of the bend created by the clockwise rotating vortex, while the fluctuation of the flag at G_y=0 is quite straight thus the value of voltage at this point.

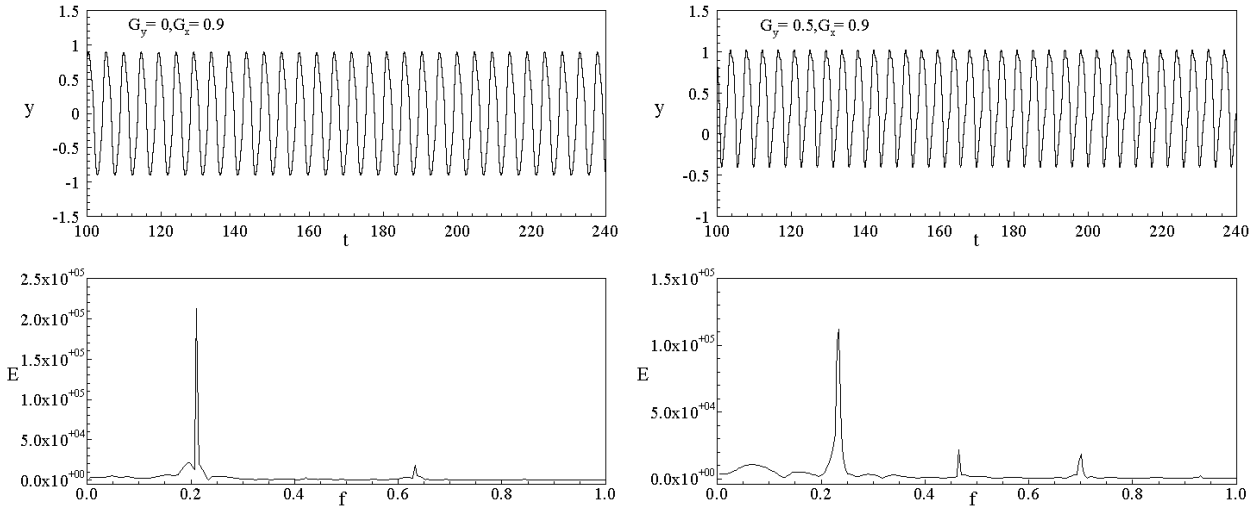

FIGURE 15. Frequency Plots for Gx=0.9 and Gy=0 and 0.5

The values of drag and voltage also shows anomaly when piezoelectric flag is place at G_x=1.0 and span wise distance is increased. The voltage contours show increasing trend as the spanwise distance is increased figure 2 (a) while the values of drag first decrease until 0.25 then start increasing until G_y=0.5 figure 2 (b)**.** At G_y=0 the flag behaves as an inverted flag (deflected mode of vibration), the vortices interaction make the flag to turn backwards and it start vibrating with very low amplitude(figure 13). The inverted flag has the highest value of the drag as it is placed in the near wake of the bluff body, but due to minimal fluctuation at this position, less amount of voltage is generated. This interaction is shown in figure 13. At G_y=0.25 the flag behaves as both inverted and conventional (biased mode of vibration) figure 13. At this point, it has a low value of drag but due to high fluctuating amplitude, it generates more energy. The dynamics of flag at G_y=0.5 is similar to the case when flag when flag was placed at G_x=0.9, G_y=0.5. The tip displacement curve and power spectrum is shown in the figure 14**,** which clearly explains the dynamic behavior of flag.

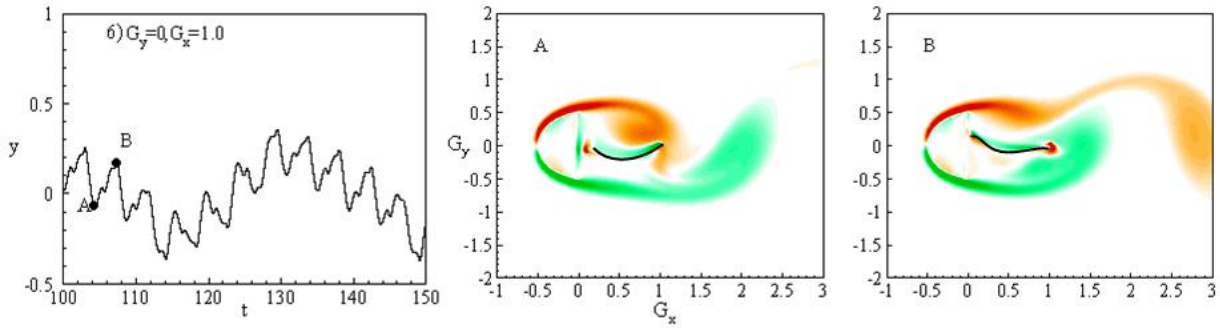

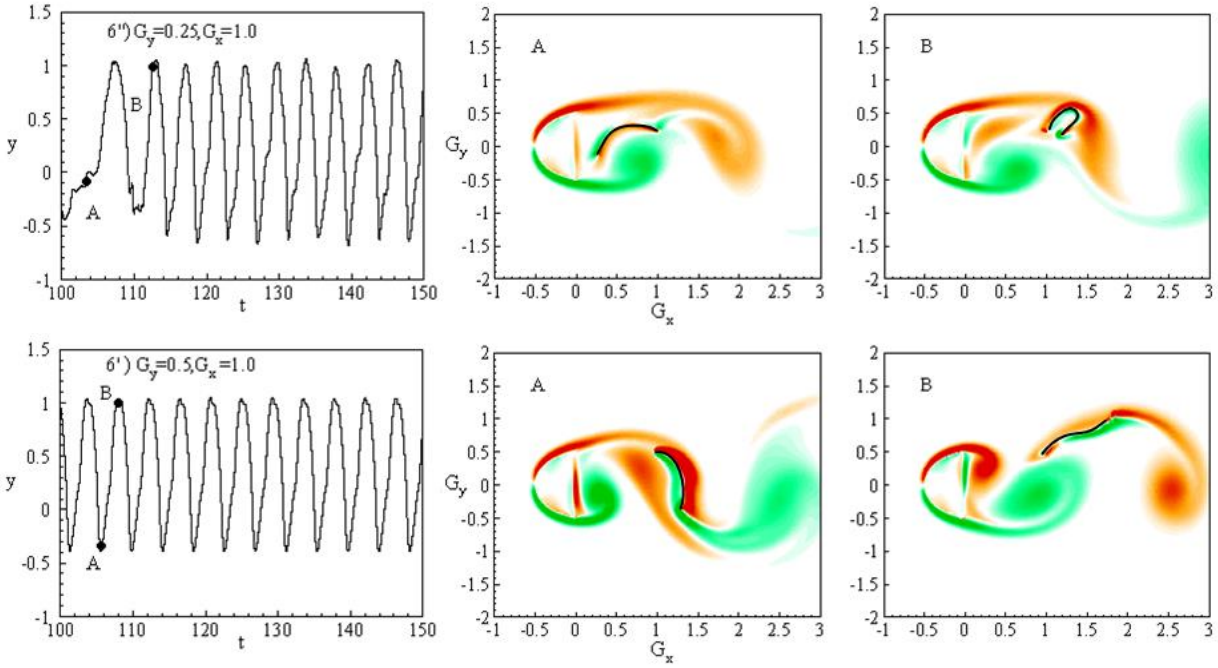

FIGURE 16. Vorticity contours around the flag for G_x=1.0 and G_y=0, 0.25 and 0.5

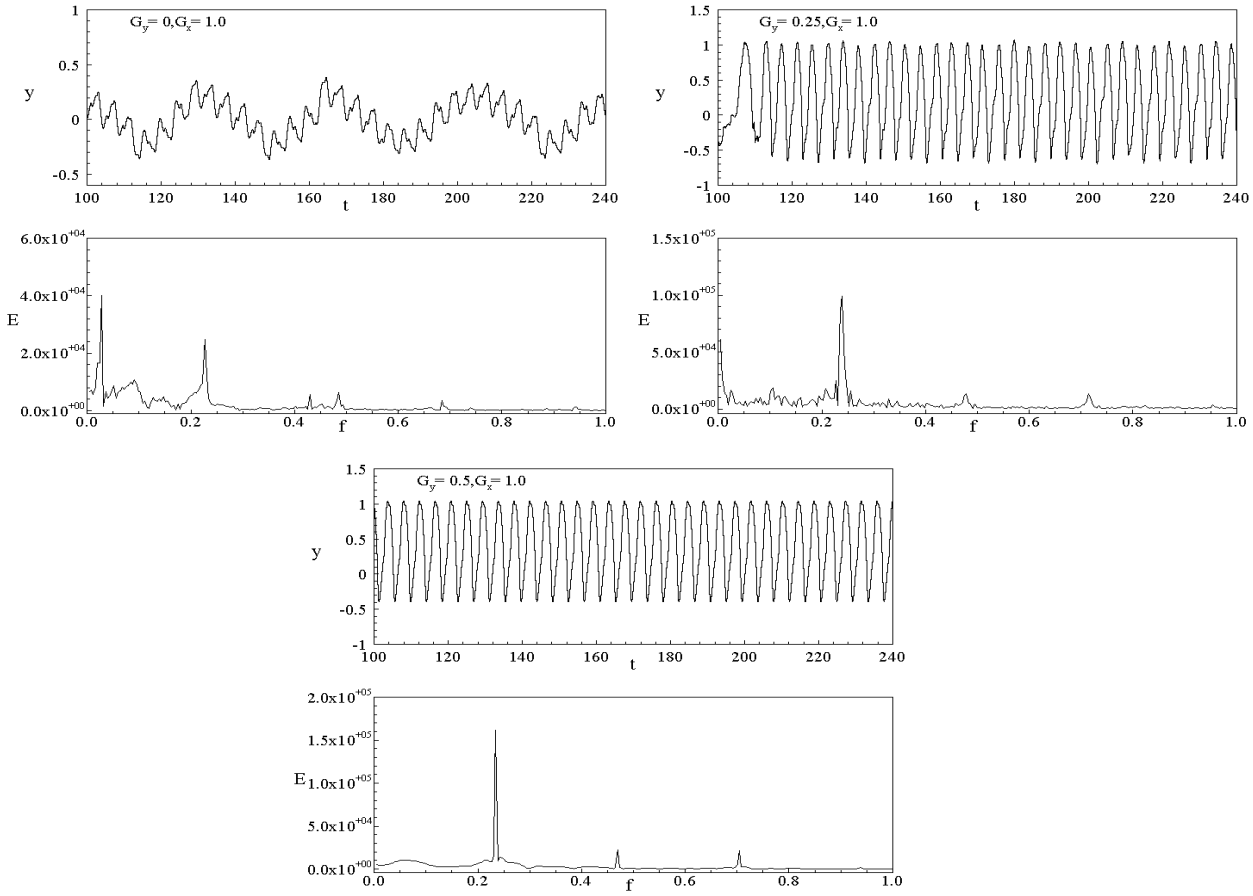

FIGURE 17. Frequency Plots for G_x=1.0 and G_y=0, 0.25 and 0.5

As the stream wise distance is further increased beyond G_x=1.2 to G_x=2.0 the voltage generated by the piezoelectric material, by changing the span wise distance remain the same as shown in figure 2 (b). However, the coefficient of drag in this region is decreasing as the span wise distance is increased from G_y=0-0.5 figure 2 (a). This decrease in the value of drag is due to irregular vortex body interaction. In this region, as the span wise distance is increased from G_y=0-0.5, the interaction of counter clockwise vortex with the flag becomes minimal. At point G_y=0.5 the counter clockwise rotating vortex leaves the flag without interacting with it, unlike case before G_x=1.2 this vortex does not strike the flag at any point and leaves the flag without having an impact on it figure 15. Due to this, the dynamics of flag is only dependent on the clockwise rotating vortices. Thus, the drag on the flag is less as compared to other cases. Although the fluid fluctuations are high resulting in the large tip displacements figure 16 which produce almost equal amount of voltage as in the cases where flag is placed at G_y=0.

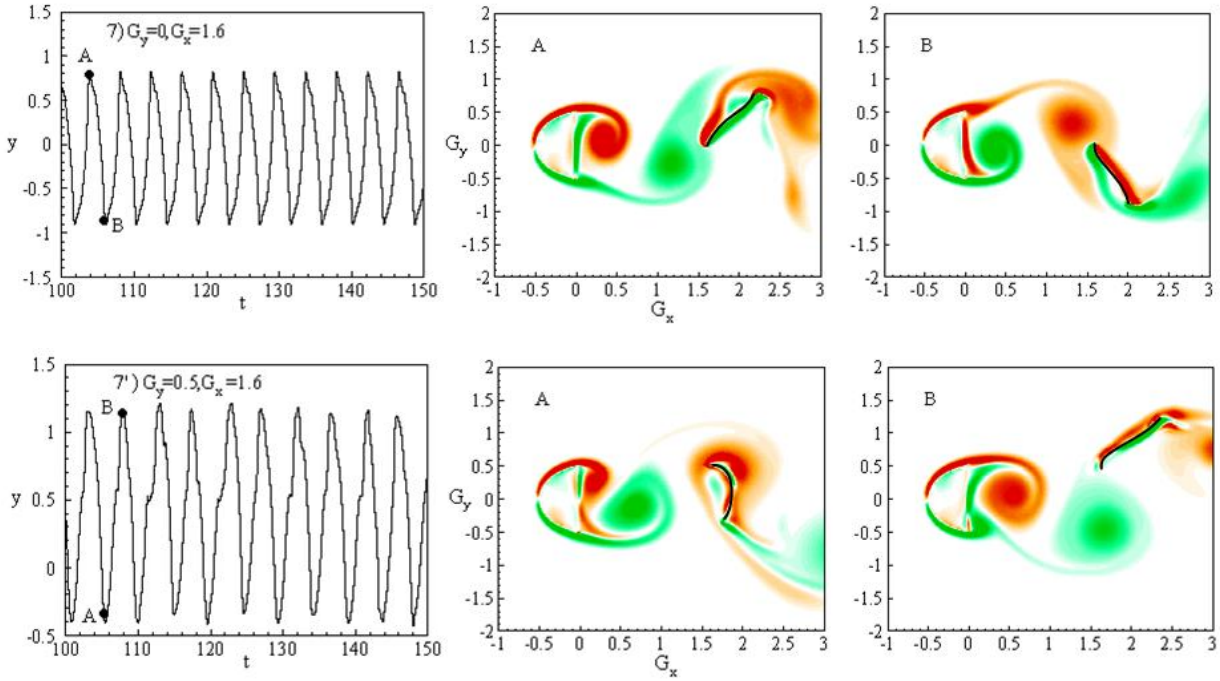

FIGURE 18. Vorticity contours around the flag for G_x=1.6 and G_y=0 and 0.5

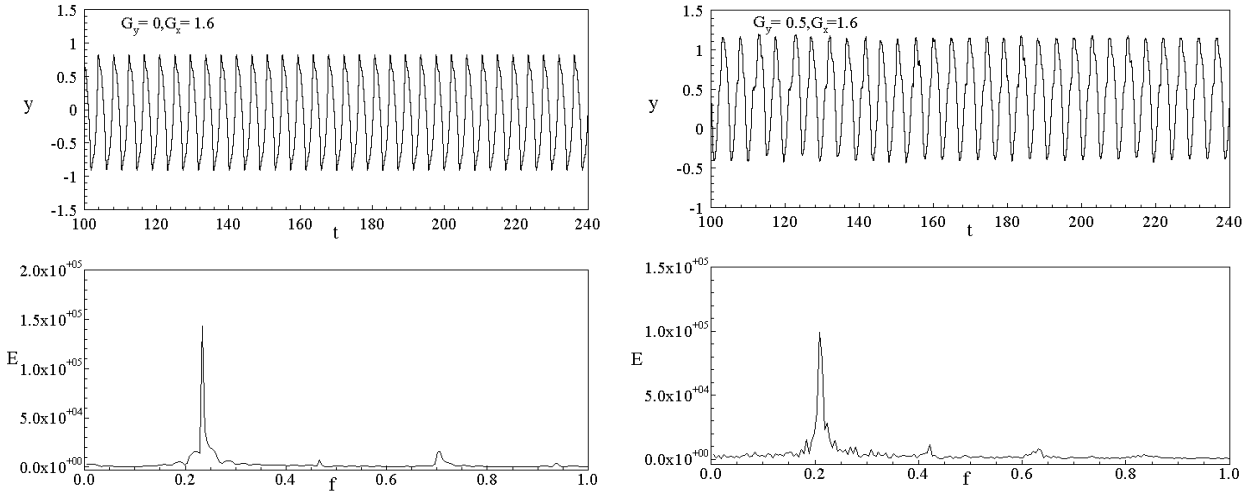

FIGURE 19. Frequency Plots for G_x=1.6 and G_y=0 and 0.5

3.2 Effect of coefficients

The purpose of this section is to understand the effects of piezoelectric parameters like coupling coefficient α and tuning coefficient β on the energy harvesting capability of piezoelectric material. In this part, we took the case where stream wise distance is changing from 0.5-2.0 at constant span wise distance. The value of tuning coefficient is taken to be constant of β=0.5 and the coupling coefficient α has been used as α=0.3 and 0.5. The coupling coefficient is dependent on the piezoelectric material properties and these values can be improved by improving the material design(Michelin & Doaré, 2013).

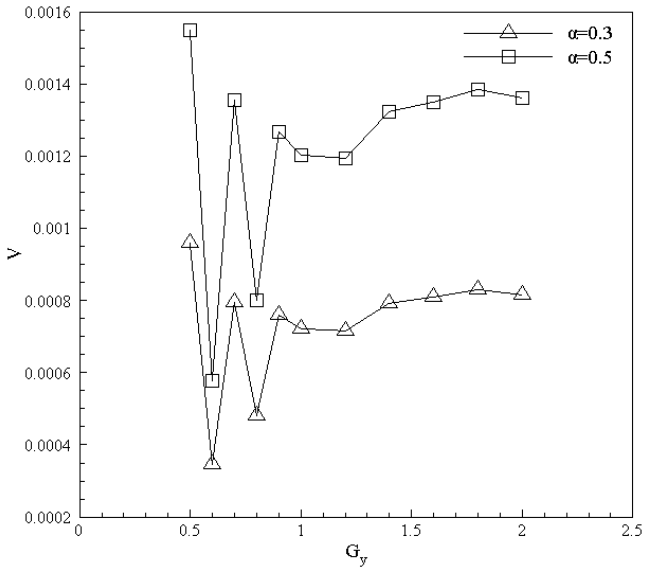

FIGURE 20. Voltage Generation at tuning coefficient Π=0.5 and coupling coefficient Ω=0.3 and 0.5

The effect of changing coupling coefficient at different stream wise distance is clearly explained by the figure 17**.** It can be seen that at different values of coupling coefficient the plot shifts upward the effect of changing the stream wise distance remains the same, but the value of the voltage generation with increase of coupling coefficient increases. It means that in future if the piezoelectric intrinsic properties of the material are improved with new immerging techniques the energy harvesting capability of piezoelectric material will increase largely, such that it may overthrow other sustainable and renewable energy sources.

3.3 Comparison with ANSYS™

In this section the results for the voltage generation form the numerical simulation are compared to the results obtained from the ANSYS™ structural. The force extracted for the numerical simulation is applied on the thin filament in the piezoelectric structural module. This force creates some disturbance in the material dipoles and energy is generated in the form of voltage.

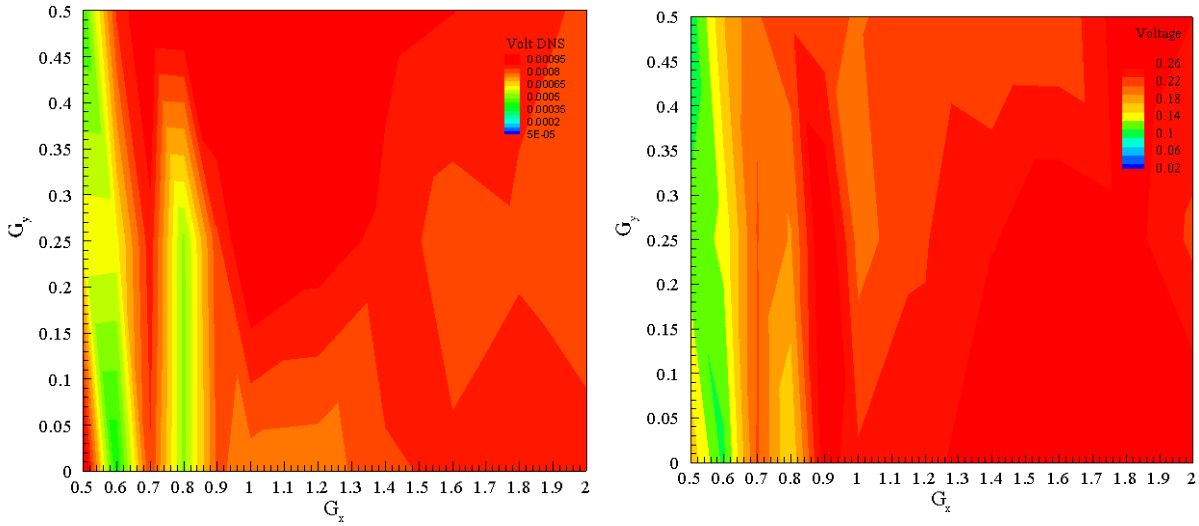

FIGURE 21. Comparison of Voltage generated by Direct Numerical Simulation (a) and Voltage generated by the ANSYS™ structural (b)

It is shown in the figure 21 that the trend of voltage generated by both methods are same at points where the flexible flag is vibrating in correspondence with the vortices generated by the D cylinder. It means that at positions G_x and G_y where the dynamics behavior of flag is smooth the result of trend voltage generation by the flag using piezoelectric extension is same as the voltage generation from the direct numerical simulation DNS.

There is off course difference in the amount of voltage that is generating from the piezoelectric flag in ANSYS™ and direct numerical simulation DNS. This is due to the fact that in ANSYS™ the flag is 3D and it is generating voltage in accordance with the dielectric and piezoelectric parameters while in DNS the voltage is generated by 2D flag in accordance with coefficient like tuning coefficient and coupling coefficient.

FIGURE 22. Comparison of ANSYS and DNS results

The difference in the both the cases for the voltage generation can be described by looking into the dynamics of the flag and bending created in the flag as the vortices are flowing over the flag. In the ANSYS™ the flag behaves as a cantilever beam in which the voltage generated by continuous vibration induced in the flag as the forces are applied on the flag, while in the other scenario, in some cases bending in the center of flag is observed and as the model is designed to calculate the voltage generation by local deformation and displacement. Due to this difference in the voltage generating methodology of the both the systems these is difference in some points as shown in the figure 21.

3.4 Conclusion

In this study, we examined the voltage generating capability of the 2 D piezoelectric flag placed in unsteady flow downstream of the D cylinder by using immersed boundary method. The fluid-solid-electric coupling is done using detailed dynamic model for dynamics of thin flexible plate. The flag is modeled as piezoelectric flag by considering it consisting of continuous small

piezoelectric patches on the surface of the flag, which convert bending deformation into electric current. The analysis was done varying the stream wise distances and span wise distance and coupling coefficient α.The conventional, biased/intermediate and deflected modes of vibration were observed and corresponded to the generation of voltage and drag of the piezoelectric flag. The values of voltage and drag changes with the change of span wise distance at particular stream wise distance, but after stream wise distance of G_x=1.2 the values of voltage are insensitive to the change in span wise distance. Although value of drag decreases at these point due to complex vortex body interaction. The increase in coupling coefficient has impact on the energy harvesting capability of the flag. The Vrms values shift from lower to high value upon increasing the coupling coefficient α, although it has no effect on the amplitude of the vibration. The voltage generation of the flag is improved if it is undergoing conventional vibration mode, the interaction of the vortices with the flag also play an important role in the energy harvesting capability of the flag. If the flag is vibrating conventionally with less bending during its vibration it will produce less voltage as compare to the movement of the flag where it is undergoing more bending deformation irrespective of amplitude, frequency and drag on the flag. Thus, increasing bending rigidity decreases the energy harvesting capability of the flag and decreasing it below a certain value decreases the stability and inertia of the flag(Doaré & Michelin, 2011)

REFERENCES

Akaydin, H. D., Elvin, N., & Andreopoulos, Y. (2010). Energy harvesting from highly unsteady fluid flows using piezoelectric materials. *Journal of Intelligent Material Systems and Structures, 21*(13), 1263-1278.

Akcabay, D. T., & Young, Y. L. (2012). Hydroelastic response and energy harvesting potential of flexible piezoelectric beams in viscous flow. *Physics of Fluids, 24*(5), 054106.

Alben, S. (2009). Simulating the dynamics of flexible bodies and vortex sheets. *Journal of Computational Physics, 228*(7), 2587-2603.

Alben, S., & Shelley, M. J. (2008). Flapping states of a flag in an inviscid fluid: bistability and the transition to chaos. *Physical review letters, 100*(7), 074301.

Allen, J., & Smits, A. (2001). Energy harvesting eel. *Journal of fluids and structures, 15*(3-4), 629-640.

Anton, S. R., & Sodano, H. A. (2007). A review of power harvesting using piezoelectric materials (2003–2006). *Smart Materials and Structures, 16*(3), R1.

Audoly, B., & Pomeau, Y. (2010). *Elasticity and Geometry*: Oxford University Press.

Bisegna, P., Caruso, G., & Maceri, F. (2006). Optimized electric networks for vibration damping of piezoactuated beams. *Journal of Sound and Vibration, 289*(4-5), 908-937.

Caliò, R., Rongala, U. B., Camboni, D., Milazzo, M., Stefanini, C., De Petris, G., & Oddo, C. M. (2014). Piezoelectric energy harvesting solutions. *Sensors, 14*(3), 4755-4790.

Connell, B. S., & Yue, D. K. (2007). Flapping dynamics of a flag in a uniform stream. *Journal of fluid mechanics, 581*, 33-67.

Curie, J., & Curie, P. (1880). Sur l'électricité polaire dans les cristaux hémièdres à faces inclinées. *CR Acad Sci Gen, 91*, 383-386.

Curie, J., & Curie, P. (1881). Contractions et dilatations produites par des tensions électriques dans les cristaux hémièdres à faces inclinées. *Compt. Rend, 93*, 1137-1140.

Doaré, O., & Michelin, S. (2011). Piezoelectric coupling in energy-harvesting fluttering flexible plates: linear stability analysis and conversion efficiency. *Journal of Fluids and Structures, 27*(8), 1357-1375.

Ducarne, J., Thomas, O., & Deü, J.-F. (2012). Placement and dimension optimization of shunted piezoelectric patches for vibration reduction. *Journal of Sound and Vibration, 331*(14), 3286-3303.

Dunnmon, J., Stanton, S., Mann, B., & Dowell, E. (2011). Power extraction from aeroelastic limit cycle oscillations. *Journal of Fluids and Structures, 27*(8), 1182-1198.

Eloy, C., Kofman, N., & Schouveiler, L. (2012). The origin of hysteresis in the flag instability. *Journal of fluid mechanics, 691*, 583-593.

Eloy, C., Souilliez, C., & Schouveiler, L. (2007). Flutter of a rectangular plate. *Journal of Fluids and Structures, 23*(6), 904-919.

Giacomello, A., & Porfiri, M. (2011). Underwater energy harvesting from a heavy flag hosting ionic polymer metal composites. *Journal of Applied Physics, 109*(8), 084903.

Gibbs, S. C., Wang, I., & Dowell, E. (2012). Theory and experiment for flutter of a rectangular plate with a fixed leading edge in three-dimensional axial flow. *Journal of Fluids and Structures, 34*, 68-83.

Guo, C. (2000). Analysis of hydroelastic instabilities of rectangular parallel-plate assemblies. *Journal of Pressure Vessel Technology, 122*(4), 502-508.

Huang, L. (1995). Flutter of cantilevered plates in axial flow. *Journal of Fluids and Structures, 9*(2), 127-147.

Huang, W.-X., Shin, S. J., & Sung, H. J. (2007). Simulation of flexible filaments in a uniform flow by the immersed boundary method. *Journal of Computational Physics, 226*(2), 2206-2228.

Huang, W.-X., & Sung, H. J. (2009). An immersed boundary method for fluid–flexible structure interaction. *Computer Methods in Applied Mechanics and Engineering, 198*(33-36), 2650-2661.

Ishihara, D., Horie, T., & Denda, M. (2009). A two-dimensional computational study on the fluid–structure interaction cause of wing pitch changes in dipteran flapping flight. *Journal of Experimental Biology, 212*(1), 1-10.

Kim, H. S., Kim, J.-H., & Kim, J. (2011). A review of piezoelectric energy harvesting based on vibration. *International journal of precision engineering and manufacturing, 12*(6), 1129-1141.

Kornecki, A., Dowell, E., & O'brien, J. (1976). On the aeroelastic instability of two-dimensional panels in uniform incompressible flow. *Journal of Sound and Vibration, 47*(2), 163-178.

Lighthill, S. J. (1975). *Mathematical biofluiddynamics*: SIAM.

Lippmann, G. (1881). Principe de la conservation de l'électricité, ou second principe de la théorie des phénomènes électriques. *Journal de Physique Théorique et Appliquée, 10*(1), 381-394.

Michelin, S., & Doaré, O. (2013). Energy harvesting efficiency of piezoelectric flags in axial flows. *Journal of Fluid Mechanics, 714*, 489-504.

Michelin, S., Smith, S. G. L., & Glover, B. J. (2008). Vortex shedding model of a flapping flag. *Journal of Fluid Mechanics, 617*, 1-10.

Nandwana, M. K., Ziaei, A., & Hansen, J. H. (2015). *Robust unsupervised detection of human screams in noisy acoustic environments.* Paper presented at the 2015 IEEE International Conference on Acoustics, Speech and Signal Processing (ICASSP).

Paidoussis, M. P. (1998). *Fluid-structure interactions: slender structures and axial flow* (Vol. 1): Academic press.

Peng, Z., & Zhu, Q. (2009). Energy harvesting through flow-induced oscillations of a foil. *Physics of fluids, 21*(12), 123602.

Pirnar, J., Dolenc-Grošelj, L., Fajdiga, I., & Žun, I. (2015). Computational fluid-structure interaction simulation of airflow in the human upper airway. *Journal of biomechanics, 48*(13), 3685-3691.

Pobering, S., & Schwesinger, N. (2004). *A novel hydropower harvesting device.* Paper presented at the 2004 International Conference on MEMS, NANO and Smart Systems (ICMENS'04).

Ramadan, K. S., Sameoto, D., & Evoy, S. (2014). A review of piezoelectric polymers as functional materials for electromechanical transducers. *Smart Materials and Structures, 23*(3), 033001.

Shelley, M. J., & Zhang, J. (2011). Flapping and bending bodies interacting with fluid flows. *Annual Review of Fluid Mechanics, 43*, 449-465.

Shoele, K., & Mittal, R. (2016). Energy harvesting by flow-induced flutter in a simple model of an inverted piezoelectric flag. *Journal of Fluid Mechanics, 790*, 582-606.

Shoele, K., & Zhu, Q. (2015). Performance of synchronized fins in biomimetic propulsion. *Bioinspiration & biomimetics, 10*(2), 026008.

Singh, K., Michelin, S., & De Langre, E. (2012a). The effect of non-uniform damping on flutter in axial flow and energy-harvesting strategies. *Proceedings of the Royal Society A: Mathematical, Physical and Engineering Sciences, 468*(2147), 3620-3635.

Singh, K., Michelin, S., & de Langre, E. (2012b). Energy harvesting from axial fluid-elastic instabilities of a cylinder. *Journal of fluids and structures, 30*, 159-172.

Taneda, S. (1968). Waving motions of flags. *Journal of the Physical Society of Japan, 24*(2), 392-401.

Tang, D., Yamamoto, H., & Dowell, E. (2003). Flutter and limit cycle oscillations of two-dimensional panels in three-dimensional axial flow. *Journal of Fluids and Structures, 17*(2), 225-242.

Tang, L., Païdoussis, M. P., & Jiang, J. (2009). Cantilevered flexible plates in axial flow: energy transfer and the concept of flutter-mill. *Journal of Sound and Vibration, 326*(1-2), 263-276.

Thomas, O., Deü, J. F., & Ducarne, J. (2009). Vibrations of an elastic structure with shunted piezoelectric patches: efficient finite element formulation and electromechanical coupling coefficients. *International journal for numerical methods in engineering, 80*(2), 235-268.

Uddin, E., Huang, W.-X., & Sung, H. J. (2013). Interaction modes of multiple flexible flags in a uniform flow. *Journal of Fluid Mechanics, 729*, 563-583.

Uddin, E., & Sung, H. J. (2012). Simulation of flow-flexible body interactions with large deformation. *International Journal for Numerical Methods in Fluids, 70*(9), 1089-1102.

Virot, E. (2015). *Flottement de drapeau: dynamique et couplage.*

Virot, E., Amandolese, X., & Hémon, P. (2013). Fluttering flags: an experimental study of fluid forces. *Journal of Fluids and Structures, 43*, 385-401.

Watanabe, Y., Suzuki, S., Sugihara, M., & Sueoka, Y. (2002). An experimental study of paper flutter. *Journal of Fluids and Structures, 16*(4), 529-542.

Wu, T. Y.-T. (1961). Swimming of a waving plate. *Journal of fluid mechanics, 10*(3), 321-344.

Zhang, J., Childress, S., Libchaber, A., & Shelley, M. (2000). Flexible filaments in a flowing soap film as a model for one-dimensional flags in a two-dimensional wind. *Nature, 408*(6814), 835.

Zhu, L., & Peskin, C. S. (2002). Simulation of a flapping flexible filament in a flowing soap film by the immersed boundary method. *Journal of Computational Physics, 179*(2), 452-468.